The FEBS Journal

FEBS PRESS science publishing by scientists

Hydrogen peroxide induces heme degradation and protein aggregation in human neuroglobin: roles of the disulfide bridge and hydrogen-bonding in the distal heme cavity

Giulia Di Rocco[1], Fabrizio Bernini[2], Gianantonio Battistuzzi[2], Antonio Ranieri[1], Carlo Augusto Bortolotti[1], Marco Borsari[2] and Marco Sola[2]

1 Department of Life Sciences, University of Modena and Reggio Emilia, Italy
2 Department of Chemical and Geological Sciences, University of Modena and Reggio Emilia, Italy

Keywords
aggregation; amyloid; electronic and MCD spectroscopies; fibril; hydrogen peroxide; neuroglobin

Correspondence
G. Battistuzzi, Department of Chemical and Geological Sciences, University of Modena and Reggio Emilia, via Campi 103, 41125 Modena, Italy
Tel: +39 0592058639
E-mail: gianantonio.battistuzzi@unimore.it
and
A. Ranieri, Department of Life Sciences, University of Modena and Reggio Emilia, via Campi 103, 41125 Modena, Italy
Tel: +39 0592058591
E-mail: antonio.ranieri@unimore.it

(Received 5 May 2022, revised 5 July 2022, accepted 20 July 2022)

doi:10.1111/febs.16581

In the present study, human neuroglobin (hNgb) was found to undergo H_2O_2-induced breakdown of the heme center at a much slower rate than other globins, namely in the timescale of hours against minutes. We investigated how the rate of the process is affected by the Cys46/Cys55 disulfide bond and the network of non-covalent interactions in the distal heme side involving Tyr44, Lys67, the His64 heme iron axial ligand and the heme propionate-7. The rate is increased by the Tyr44 to Ala and Phe mutations; however the rate is lowered by Lys67 to Ala swapping. The absence of the disulfide bridge slows down the reaction further. Therefore, the disulfide bond-controlled accessibility of the heme site and the residues at position 44 and 67 affect the activation barrier of the reaction. Wild-type and mutated species form β-amyloid aggregates in the presence of H_2O_2 producing globular structures. Furthermore, the C46A/C55A, Y44A, Y44F and Y44F/C46A/C55A variants yield potentially harmful fibrils. Finally, the nucleation and growth kinetics for the aggregation of the amyloid structures can be successfully described by the Finke–Watzky model.

Introduction

In recent years, the neuroprotective role of human neuroglobin (hNgb) under conditions of oxidative stress has increasingly clearly been recognized [1–9]. hNgb is one of the most interesting members of the six-coordinate His/His-ligated heme *b*-containing class of globins found in the last two decades in different organisms, including mammals, avians, fishes and amphibians [2,3,9]. hNgb is a 17-kDa monomer featuring a typical globin fold [2,10–13] despite < 30% sequence identity with myoglobin (Fig. 1) [2,12–14]. The six-coordinate (His96/His64)-axially ligated form of hNgb is in equilibrium with a minor five-coordinate species in which His64 is detached from the iron atom. hNgb is abundant in the neurons of the hypothalamus and in the retinal cells (with concentrations up to 100 μM [15]), whereas it is present at a relatively low concentration (approximately 1 μM) in other parts of the central nervous system [16–24] and in

Abbreviations
AFM, atomic force microscopy; ATR-FTIR, attenuated total reflectance-FTIR; hNgb, human neuroglobin; ROS, reactive oxygen species; ThT, thioflavin T.

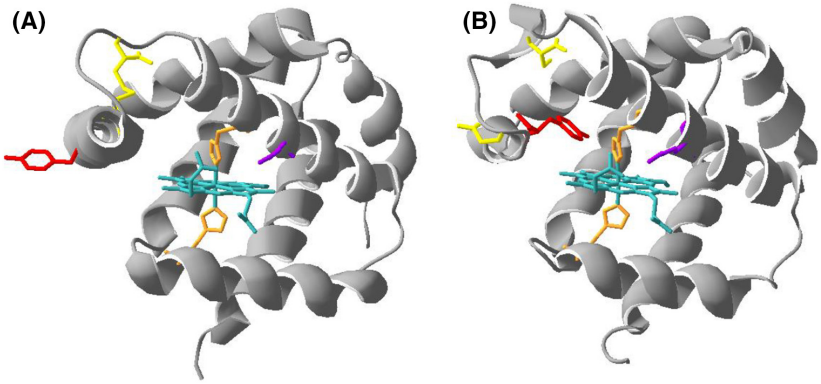

Fig. 1. Cartoon representation of the structure of (A) wt hNgb (4mpm.pdb, chain A) featuring the disulfide bridge between Cys46 and Cys55 and of (B) the C46/C55S mutant of hNgb (1oje.pdb, chain B) without the disulfide bridge between Cys46 and Cys55. The heme group and the iron axial ligands His 64 and His 96 are represented in light blue and orange, respectively, whereas the residues that were mutated in the present study are represented in yellow (Cys 46 and Cys 55), red (Tyr 44) and violet (Lys 67).

non-neuronal tissues such as the heart, gastrointestinal tract, haematopoietic stem cells, tumoral cells and endocrine tissues [2,4,18,20,25–28]. The physiological role of hNgb remains an issue [2,3,9,29]. The six-coordinate heme iron and the high rate of autooxidation of the ferrous heme rule out its involvement in the storage/transport of O_2 (and other ligands) typical of ordinary 5-coordinate globins, although its function as O_2 supplier to the nerve cells with respect to protecting them in case of hypoxia and ischemia has been proposed [2,9,15,28,29]. Strong evidence has been gained indicating that *in vivo* hNgb is overexpressed under conditions of oxidative stress, hypoxia and glucose deficiency, thereby suggesting a neuroprotective function, although this remains debated [1–4,6–9,29,30]. In particular, hNgb overexpression would protect neurons from mitochondrial dysfunctions [2,7–9,31,32] and neurodegenerative disorders, such as Alzheimer's disease [2,9,33–36]. Other possible functions include scavenging of dangerous reactive nitrogen species and reactive oxygen species (ROS) and the conversion of harmful surplus of NO to NO_3^- [37–40] and also the production of NO from NO_2^- for signalling events [39,41–44]. Moreover, hNgb reduces the ferric cytochrome *c* released in the cytosol, thus preventing apoptosis induced by the oxidative stress [2,9,24,45–51]. Interestingly, because H_2O_2-induced heme degradation in Ngb is considerably slower compared to other heme proteins, it has been converted into multifunctional enzymes that are capable of catalyzing dye-decolorization and dehalogenation reactions using H_2O_2 as an oxidant [52,53].

In the present study, we investigated the interaction of hNgb with hydrogen peroxide, the paradigmatic ROS [54], aiming to gain information on the response of this protein to an oxidizing agent that is easily formed under oxidative stress conditions. These findings may help our understanding of one important action underlying the protective role of this species against oxidative cell damage. We tackled this problem by investigating the native protein and a few mutants on key residues affecting the protein environment and the accessibility of the heme center to solvent. In particular, the double mutant C46A/C55A lacks the intramolecular disulfide bridge between these cysteine residues that forms under oxidizing conditions and is considered a determinant of the functional regulation of the protein [2,55–65]. Removal of the disulfide bridge results in the strengthening of the axial heme iron bond with the distal His64 and the partial closure of the heme crevice. These changes decrease heme accessibility to solvent that in turn lowers the affinity of hNgb for exogenous ligands, such as O_2, NO_2^- and CN^- [41,42,44,55,59,60,65,66]. Conversely, the presence of the disulfide bridge significantly increases hNgb affinity for exogenous ligands as well as its activity as NO_2^- reductase [42]. Tyr44 and Lys67 are other key residues located in the heme distal side (Fig. 1). In the absence of the disulfide bridge, they take part in a hydrogen-bonding and electrostatic network also involving the distal His64 and the heme propionate 7 [12,59], which stabilizes the heme environment and limits the access of exogenous ligands to the heme iron providing an energy barrier for ligand binding prior to detachment of the distal His64 [67–70]. Here, we replaced Tyr44 with an Ala and a Phe residue. Both variants lack the hydrogen-bonding network yielded by Tyr44 in wild-type (wt) hNgb, but

differ in the steric hindrance of the substituting residue. The Y44A mutation would induce a larger accessibility of the distal heme side to solvent and exogenous ligands. Upon formation of the C46–C55 intramolecular disulfide bridge, Tyr44 moves out of the heme cavity [12,59]. Therefore, we investigated the effect of these Tyr44 replacements on the interaction with H_2O_2 in the presence and absence of the above-mentioned disulfide bridge by examining the single Y44A and Y44F variants and the triple Y44A/C46A/C55A and Y44F/C46A/C55A variants, respectively. Similarly, we examined the K67A and K67A/C46A/C55A variants. Moreover, we focused on the impact of these mutations on the H_2O_2-induced protein aggregation and fibril formation. Ngb shows a certain ability to form amyloid fibrils spontaneously both in apo and holo form, even if with very slow kinetics [71]. The nucleation and growth kinetics of the protein aggregates were found to follow the Finke–Watzky model [72,73]. Overall, these mutations demonstrate that the architecture of the distal site of hNgb controls the kinetics and thermodynamics of the hydrogen peroxide-induced heme breakdown and protein aggregation.

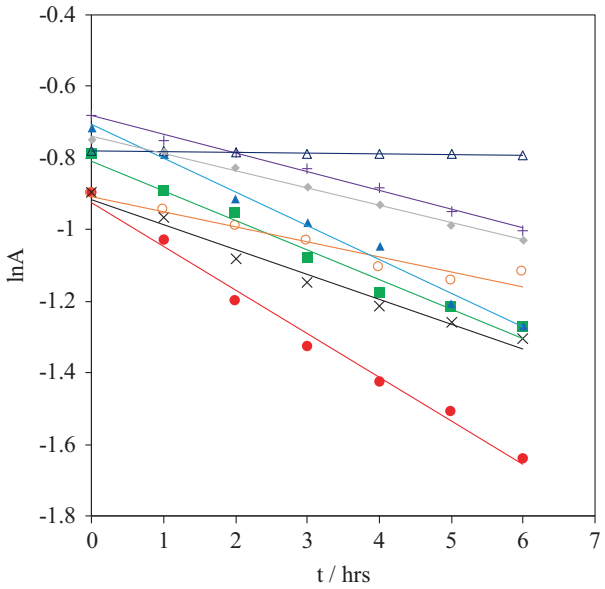

Fig. 2. Plot of the absorbance of the Soret band at 413 nm vs. time in the presence of 200 μM H_2O_2: (■) wt, (●) Y44A, (▲) Y44F, (×) K67A, (+) C46AC55A, (○) Y44A/C46A/C55A, (△) Y44F/C46A/C55A and (◆) K67A/C46A/C55A. Protein concentration: 3–5 μM, 10 mM phosphate buffer plus 0.1 M NaCl (pH 7.4). T = 298 K. The same plots in the presence of 50 μM H_2O_2 are shown in Fig. S3.

Results

Effects of hydrogen peroxide on the electronic absorption spectra of wt and mutated hNgb

The absorption spectra of all species are almost identical and typical of a six-coordinate ferric heme as indicated by the Soret band at 413 nm and the Q bands at 532 and 554(sh) nm (Fig. S1) [10,38,39]. In all cases, no five-coordinate heme-containing species were detected consistent with the low abundance (< 5%) of this form at neutral pH [74]. The Soret bands recorded over time after addition of 50 and 200 μM H_2O_2 are shown in Fig. S2. These H_2O_2 concentrations mimic a chronic/prolonged (timescale of days) and acute/transitory (timescale of minutes/hours) condition of extracellular oxidative stress, respectively [75]. The intensities of the Soret and the Q bands decrease to zero with time (Figs S1 and S2). No changes in wavelength and shape are observed, as well as no appearance of new signals. These results indicate that H_2O_2 causes progressive heme degradation. After about 30 h, the formation of a white milky precipitate is observed.

The time course of the intensity decrease follows a pseudo first-order kinetics (Fig. 2 and Fig. S3). The kinetic constants are listed in Table 1. Heme degradation is faster in 200 μM H_2O_2 compared to 50 μM H_2O_2, whereas, for a given H_2O_2 concentration, it slows down for the variants lacking the disulfide bridge (namely bearing the C46A/C55A mutations). Moreover, in these mutants, the Tyr44 to Ala and Phe and the Lys67 to Ala mutations exert a rate-decreasing effect. By contrast, in the presence of the disulfide bridge, the reaction rate is increased by the Tyr44 to Ala and Phe mutations and decreased upon replacement of Lys67 with Ala.

Table 1. Pseudo first-order kinetic constants for H_2O_2-induced heme degradation for wt hNgb and its mutants in the presence of 50 and 200 μM H_2O_2. Values were obtained from the plots shown in Fig. 2 and Fig. S3. The k values are affected by an error of about ±0.005 h^{-1}. Protein concentration: 3–5 μM, 10 mM phosphate buffer plus 0.1 M NaCl (pH 7.4). T = 298 K.

hNgb	k_{50}/h^{-1}	k_{200}/h^{-1}
wt	0.083	0.170
C46A/C55A	0.052	0.112
Y44A	0.122	0.236
Y44A/C46A/C55A	0.042	0.090
Y44F	0.094	0.189
Y44F/C46A/C55A	0.002	0.004
K67A	0.069	0.139
K67A/C46A/C55A	0.048	0.104

Effects of hydrogen peroxide on the aggregation of wt and mutated hNgb Attenuated total reflectance-FTIR (ATR-FTIR) and thioflavin fluorescence spectra in the presence of H_2O_2

The ATR-FTIR spectra of all species (Fig. S4) contain a single band for both Amide I and Amide II vibrational modes. The Amide I band (1600–1700 cm^{-1}) originates for the most part from the stretching of the peptide C=O bonds of the protein backbone and is particularly sensitive to the amount of the various secondary structure motifs [76–78]. Amyloid fibrils show a characteristic band clustering between 1611 and 1630 cm^{-1}, whereas, for native β-sheet proteins, it is observed from 1630 to 1643 cm^{-1} [79]. For all species, H_2O_2 induces a broadening of the Amide I band that also becomes less symmetric, particularly in the lower wavenumber region, indicative of changes in the secondary structure. The second-derivative spectra were calculated in the absence of hydrogen peroxide and after 24 h of incubation with 200 μM H_2O_2 (Fig. S5). Those obtained after incubation with H_2O_2 always show a significant increase in the signal in the region around 1620–1630 nm (not observed or negligible in the absence of H_2O_2), suggesting the formation of β-sheet structures of amyloid type [76–78].

Thioflavin T (ThT) is a widely exploited molecular probe used to investigate the mechanism of formation of β-amyloid aggregates. ThT binding to β-sheet-containing structures, such as amyloid fibrils, is highly specific and induces a blue-shift of the ThT fluorescence band maximum from 510 nm to 480–490 nm accompanied by an intensity increase [80,81]. ThT added to hNgb and the present variants shows the fluorescence spectrum typical of the unbound form even after 24 h of incubation. By contrast, for all species, addition of H_2O_2 results in the appearance and progressive growth of the 485 nm band typical of the presence of amyloid aggregates (Fig. 3). The time course of such an intensity increase is shown in Fig. 4. Unfortunately, protein precipitation occurring after about 30 h incubation causes a fast decrease in the intensity of the fluorescence emission and prevents observation of the plateau phase corresponding to the end point for the conversion of the protein into amyloid aggregates.

The C46A/C55A, Y44A and Y44A/C46A/C55A variants feature a sort of induction time, followed by fast amyloid formation, whereas the wt, Y44F and Y44F/C46A/C55A variants show a more progressive fluorescence increase, and the K67A and K67A/C46A/C55A variants show almost no band formation. Invariably, the experimental data fit well with those calculated by applying the Finke–Watzky model (Fig. 4). Such a two-step model for aggregate formation assumes a first

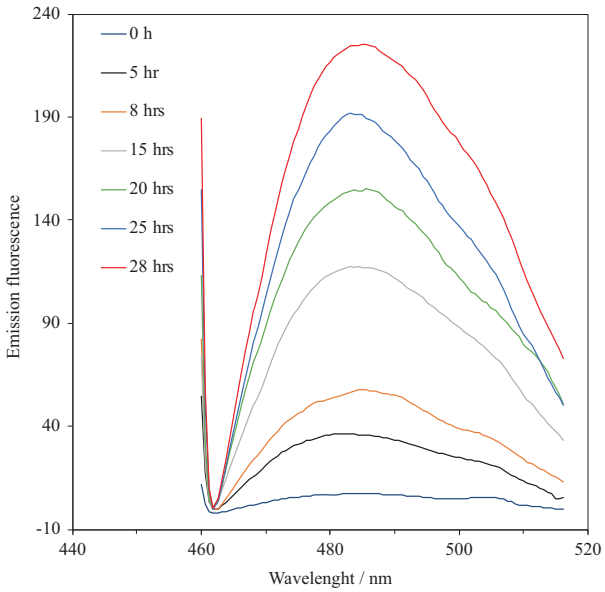

Fig. 3. Time course of the thioflavin T (ThT) fluorescence spectrum in the presence of wt hNgb upon addition of 200 μM H_2O_2. The variants show a similar behaviour. Excitation at 450 nm, ThT concentration: 20 μM; protein concentration: 5 μM, 10 mM phosphate buffer plus 0.1 M NaCl (pH 7.4). T = 298 K.

nucleation step followed by an autocatalytic growth at the surface, namely [72,73]:

$$nA \xrightarrow{k_1} B_n \quad n > 2$$

$$B_n + A \xrightarrow{k_2} B_{n+1}$$

where A is the monomer and B_n is the oligomer formed by nucleation, which grows autocatalytically. A number of protein aggregation events leading to neurological diseases involving amyloid (Alzheimer's disease), α-synuclein (Parkinson's disease) and polyglutamin (Huntington's disease) follow the kinetic law obtained from this model (Eqns 1–3) [73]:

$$-d[A]/dt = k_1[A] + k_2[A][B_y] \quad B_y = \sum_n B_n, \qquad (1)$$

$$[A]_t = \left[(k_1/k_2) + [A]_0\right] / \left[1 + (k_1/k_2[A]_0) \exp\left[(k_1 + k_2[A]_0)t\right]\right] \qquad (2)$$

$$[B]_t = [A]_0 - \left[(k_1/k_2) + [A]_0\right] / \left[1 + (k_1/k_2[A]_0) \exp\left[(k_1 + k_2[A]_0)t\right]\right] \qquad (3)$$

The k_1 and k_2 values obtained from the data fit are listed in Table 2.

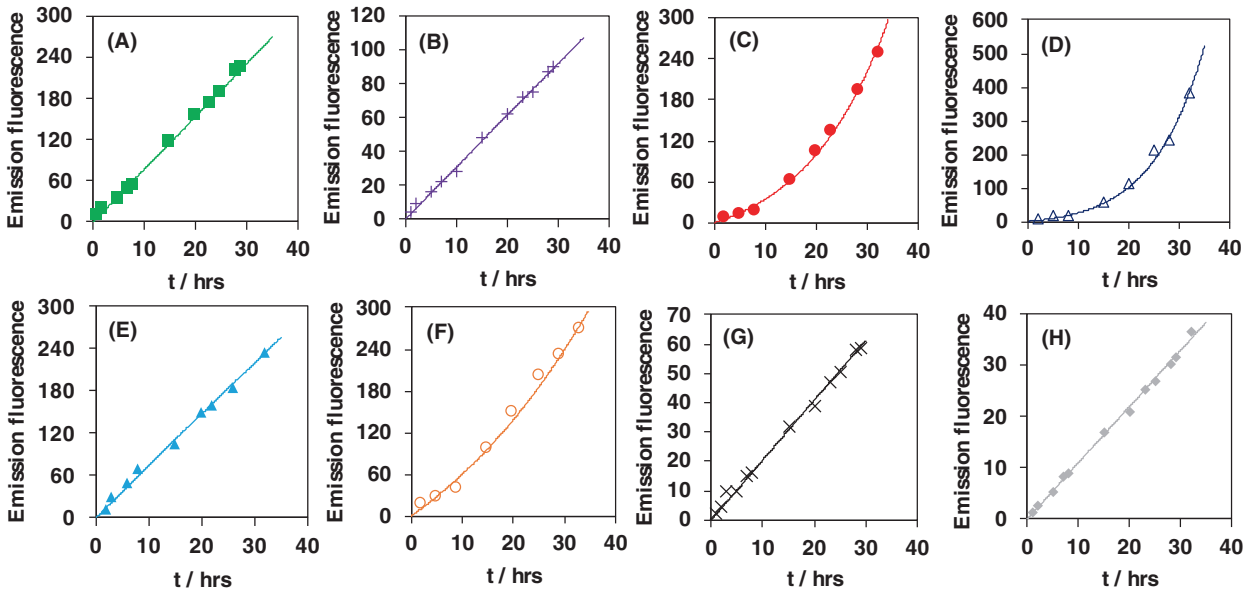

Fig. 4. Plot of the ThT fluorescence emission intensity of the 485 nm band vs. time upon addition of 200 μM H_2O_2: (A) wt, (B) C46AC55A, (C) Y44A, (D) Y44AC46AC55A, (E) Y44F, (F)Y44FC46AC55A, (G) K67A and (H) K67AC46AC55A. ThT concentration: 20 μM; protein concentration: 5 μM, 10 mM phosphate buffer plus 0.1 M NaCl (pH 7.4). $T = 298$ K. Continuous lines are the best fit curves based on the Finke–Watzky model [72,73].

Atomic force microscopy (AFM) study of protein aggregates

In the absence of H_2O_2, no significant aggregates on mica surface are detected for all species within 24 h. By contrast, protein aggregates form after 24 h of incubation with 200 μM H_2O_2. The AFM images are shown in Fig. 5 and Fig. S6. wt hNgb yields several small globular aggregates, often poorly defined, but no fibrils. Their largest height is 0.45 nm, although the large majority of the aggregates do not exceed 0.2 nm (Fig. S7). The C46A/C55A variant lacking the disulfide bridge also shows numerous small aggregates, most of which are about 1.1–1.2 nm (maximum of 2 nm) in height; however, a few well developed fibrils are observed with a height between 2.0 and 2.1 nm and lengths from 200 to 300 nm (Fig. S7). The Y44A variant, instead, forms well defined and large globular aggregates (2.5–3.5 nm, maximum of 8 nm in height), but also agglomerate structures and squat fibrillary bodies, mostly aggregated, the latter with heights between 2.5 and 3.5 nm and lengths from 50 to 100 nm (Fig. S7). The variant containing the same mutation but deprived of the disulfide bridge, namely Y44A/C46A/C55A, yields large and well defined globular aggregates as described above (average 4 nm, maximum of 8 nm in height), some rare agglomerate structures but no fibrils at all (Fig. S7). Insertion of a Phe in place of Tyr44 in the Y44F variant yields longer fibrils compared to Y44A. In particular, the globular aggregates are numerous and smaller than above (average height of 2.0–2.5 nm), although well developed and often overlapped fibrillary structures are observed, 2.0–2.5 nm high and lengths on average

Table 2. Kinetic constants for H_2O_2-induced nucleation (k_1) and autocatalytic growth at a surface (k_2) for wt hNgb and its mutants according to the Finke–Watzky model [72,73]. Values were obtained from the plots shown in Fig. 4. The k values are affected by a relative error of about ±8%. Protein concentration: 3 μM, 10 mM phosphate buffer plus 0.1 M NaCl (pH 7.4). $T = 298$ K. For sake of comparison, the kinetic data for aggregation of $A\beta_{42}$, α-synuclein and polyglutamin are reported from Morris *et al.* [73].

hNgb	k_1/h^{-1}	$k_2/mM^{-1}\cdot h^{-1}$
wt	1.52×10^{-3}	0.51
C46A/C55A	0.62×10^{-3}	0.51×10^{-2}
Y44A	0.49×10^{-3}	13.1
Y44A/C46A/C55A	0.29×10^{-3}	21.7
Y44F	1.50×10^{-3}	0.11×10^{-2}
Y44F/C46A/C55A	1.05×10^{-3}	5.61
K67A	0.41×10^{-3}	0.72×10^{-2}
K67A/C46A/C55A	0.22×10^{-3}	0.37×10^{-2}
$\alpha\beta_{42}$	1.0×10^{-4}	5.7×10^{-2}
$\alpha\beta_{42}$ + Zn(II)	8.3×10^{-4}	6.3×10^{-2}
α-Synuclein	0.48×10^{-4}	40
Polyglutammine	2.6×10^{-3}	2.3×10^{-2}

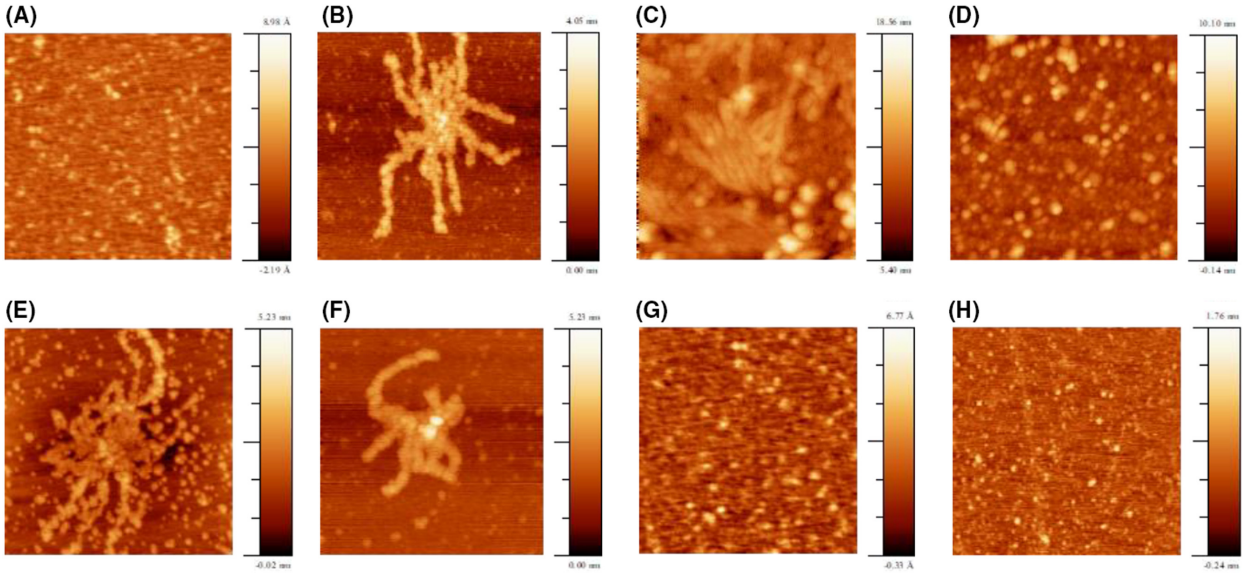

Fig. 5. Topographic AFM images of protein aggregates formed by hNgb and variants subjected to incubation with H_2O_2: (A) wt, (B) C46AC55A, (C) Y44A, (D) Y44AC46AC55A, (E) Y44F, (F) Y44FC46AC55A, (G) K67A and (H) K67AC46AC55A. Protein samples (5 μM in 10 mM phosphate buffer plus 0.1 M NaCl, pH 7.4, and 200 μM H_2O_2) were aged at 20 °C in the dark for 24 h.

> 200 nm that can reach up to 500 nm (Fig. S7). Upon cleavage of the disulfide bond in the Y44F/C46A/C55A variant only minor changes are observed. In particular, the globular aggregates are lower (average height 1.0–1.2 nm) such as the fibrillary structures (1.2–1.6 nm), which show lengths from 300 to slightly above 500 nm (Fig. S7). Similar to wt hNgb, both K67A and K67A/C46A/C55A yield small globular aggregates (with an average height of 0.3–0.4 nm and 1–1.2 nm for K67A and K67A/C46A/C55A, respectively), but no fibrils (Fig. S7).

Discussion

Kinetics and mechanism of H_2O_2-induced heme degradation in hNgb

The mechanism of H_2O_2-induced oxidative degradation of the heme center in globins starts with the formation of a Fe(III)-hydroperoxide intermediate that yields the α-meso-hydroxy-heme group, which then evolves in verdoheme (upon CO release) and afterwards is further oxidized to biliverdin [82–88]. One of the physiological roles hypothesized for hNgb is the protection of the neuron and retinal cell from oxidative stress with an as yet unknown mechanism [1–4,6–8,29,30,38,89] that, as for the other globins [90–93], could involve heme degradation. The generally accepted mechanism by which pentacoordinate globins, such as myoglobin and haemoglobin, react with hydrogen peroxide [82,83] involves the oxidation of the ferrous or ferric heme of the globin by hydrogen peroxide (or peroxides) to a ferryl species. The latter, unlike the true peroxidase enzymes, is very unstable and, in the absence of substrate, leads to oxidative modifications or degradation of the heme itself or the protein. The proposed protective role of hNgb, however, would conflict with its documented resistance to the oxidative stress attributed to the unfavored formation of the ferryl heme center as a result of the presence of the two axial His ligands to the heme iron [38,94]. However, we note that the above finding is based on experiments in which relatively brief reaction times of hNgb with H_2O_2 were allowed (< 1 h) [38,94]. This timescale was chosen by analogy to myoglobin and haemoglobin that react completely with H_2O_2 within minutes [83,95–99]. In hNgb, the six-coordinate heme center and the steric hindrance of the polypeptide matrix surrounding the heme make the heme center scarcely accessible and reactive to exogenous ligands. Here, we found that these features do not prevent heme degradation and subsequent iron ion release by H_2O_2 but make it dramatically much slower compared with the other globins. Moreover, the reaction rate is affected by mutation of both Tyr44 and Lys67. Indeed, the pseudo first-order kinetic constants obtained from the time course of the H_2O_2-induced bleaching of the Soret band (Fig. 2 and Table 1) decrease in the order: Y44A > Y44F > wt > K67A > C46A/C55A > K67A/C46A/C55A > Y44A/C46A/C55A> > Y44F/C46A/C55A for both H_2O_2 concentrations investigated. The last

mutant is particularly resistant to the oxidative action of H_2O_2, showing a very limited heme degradation even after 24 h. These mutational effects on the kinetic constants could be related to the accessibility of the heme center to solvent, for which the decrease is expected to slow down heme degradation. Indeed, heme accessibility is reduced by the removal of the disulfide bridge as it closes the heme crevice, and it is also affected by the steric hindrance and the arrangement of the Tyr44 and Lys67 side chains. A rough correlation can be established between the kinetic constants and the volume of the heme crevice (Fig. S8). Y44F/C46A/C55A is a clear outlier and the other data are rather scattered, suggesting that other factors also control the rate of the oxidative heme degradation. Indeed, the kinetic constants must also conceivably be related to the amount of five-coordinate heme center, which is the only species able to interact with H_2O_2 to yield the hydroperoxo derivative and eventually the ferryl center needed for heme degradation. Such a content is known to decrease with removal of the disulfide bridge and may also be subjected to mutational effects [12,57,62]. In addition, other factors, such as the availability of residues able to form hydrogen bonds and the presence of hydrophobic regions in the heme pocket, could play a relevant role.

We note that the kinetic constants for 200 μM H_2O_2 are approximately twice those for 50 μM H_2O_2. Therefore, despite only two data points being available, it is unlikely that the reaction is of the first order with respect to H_2O_2. Therefore, the mechanism of heme oxidation by H_2O_2 is complex. Here, neither hydroperoxide nor verdoheme intermediates (showing absorptions at about 700 nm) typical of heme breakdown for the other globins and heme proteins [100,101] have been observed in the UV-visible spectra of hNgb incubated with H_2O_2. However, these bands could be low-intensity because of the kinetic lability of these species and the slowness of the first oxidation step, which does not allow the accumulation of the reaction intermediates. Accordingly, we note that a broad feature at about 700 nm appears with time in the second derivative spectra of hNgb in the presence of H_2O_2 (Fig. S9). Therefore, the presence of the verdoheme intermediate in the heme breakdown of hNgb cannot be excluded [96]. Its concentration during the reaction could be small as a result of its fast transition to biliverdin. These observations suggest that the heme group of hNgb undergoes H_2O_2-induced oxidative degradation, possibly sharing the mechanism of the other globins, although it features a larger resistance that is kinetic in nature because the process is much slower.

Aggregation of hNgb upon H_2O_2-induced heme breakdown

Ngb is capable of spontaneously forming amyloid fibrils with very slow kinetics [71]. In the presence of H_2O_2, however, the rate of this process increases considerably and is a function of residue replacement around the heme center. For all of the investigated species, the β-sheet content is negligible or very low, as can be seen from the second-derivative AT-FTIR spectra (Fig. S5). Such content increases upon H_2O_2 addition and the consequent protein aggregation. The ThT fluorescence spectra indicate the formation of amyloid type structures for which aggregation kinetics differ for the various species (Figs 3 and 4 and Table 2). The k_1 values are rather similar, whereas the k_2 values are affected by some mutation-induced differences. The presence of the disulfide bridge does not affect the kinetics of amyloid formation (Table 2). Moreover, the k_1 and k_2 values do not correlate with the ability of the protein to yield fibrils: indeed, the species that do not produce fibrillar structures (wt, Y44A/C46A/C55A, K67A and K67A/C46A/C55A) show kinetic constants that are scattered within the protein series.

AFM measurements (Fig. 5 and Fig. S6) show that fibrils are formed by Y44F, Y44F/C46A/C55A, Y44A and C46A/C55A incubated with 200 μM H_2O_2. The disulfide bridge does not exert a univocal effect on fibril formation and there is no relationship between the yield of the aggregates and their morphology. wt hNgb produces amyloid aggregates with a high yield but these do not organize to yield fibrils. They do so only in the absence of the disulfide bridge (the C46/C55 variant), namely under reducing instead of oxidizing conditions. Consistently, the formation or breaking of a disulfide bridge has often been closely associated with amyloid formation for several proteins. [102–105]. Interestingly, the Y44F/C46A/C55A, although showing very slow oxidation kinetics, yields similar amount of fibrillary structures within the same time scale compared to wt Ngb and the other mutants. This can tentatively be related to the formation of mixed fibrillary structures involving both degraded and intact species, with the former acting as sort of aggregation promoter [106–108].

Fibrils are responsible of plaque formation in Alzheimer's disease and other neurodegenerative diseases. However, we note that the mutants studied here, although presently not included among those possessing a physio-pathological relevance [2], do yield fibrils if subjected to oxidative stress. Therefore, ROS could in principle poise other as yet unknown hNgb mutants for β-amyloid fibril formation.

Conclusions

The present study provides compelling evidence indicating that hNgb is more resistant to the oxidative action of H_2O_2 compared to the other globins (i.e. haemoglobin and myoglobin), but is nonetheless subjected to heme breakdown, although at a much slower rate. Such behaviour is related mainly to the presence of a heme center in equilibrium between a largely prevailing six-coordinated state and a five-coordinated one. The reaction with H_2O_2 is slower for the former state compared to the latter because of the need for ligand substitution. The absence of the disulfide bond in the variant containing the C44A and C55A mutations results in a further lowering of the reaction rate because of the conformational rearrangement that decreases the solvent accessibility of the heme center. wt Ngb and all of the variants investigated here yield β-amyloid aggregates in the presence of H_2O_2. However, only the aggregates formed by the Y44F and Y44A variants evolve towards the production of fibrils, whereas the wt variant only does so upon cleavage of the disulfide bridge. It therefore appears that hNgb behaves like a two-faced Janus. On the one hand, under conditions of chronic oxidative disorders, it may undergo heme degradation, thereby consuming ROS and protecting the cell from further damage. On the other, if the disulfide bridge breaks or some mutated form are present, it may aggregate to form β-amyloid fibrils that produce plaques, thereby contributing to the onset of Alzheimer's disease or retinal amyloidosis.

Materials and methods

Materials

All chemicals were reagent grade. Tris(hydroxymethyl)aminomethane (Tris) was purchased from Sigma-Aldrich (St Louis, MO, USA). Sodium mono-hydrogen phosphate, sodium di-hydrogen phosphate, sodium chloride and sodium perchlorate were purchased from Carlo Erba Reagenti (Milan, Italy). Water was purified through a Milli-Q Plus Ultrapure Water System coupled with an Elix-5 Kit (Millipore, Burlington, MA, USA). The water resistivity was > 18 MΩ cm.

Protein expression and isolation

hNgb (GeneBank reference sequence AF422796) was expressed in *Escherichia coli* as reported previously [56]. The synthetic genes for all the Ngb variants (Y44A, Y44F, K67A, C46A/C55A, Y44A/C46A/C55A, Y44F/C46A/C55A and K67A/C46A/C55A) were purchased from Integrated DNA Technologies (Coralville, IA, USA) and subcloned in the prokaryotic expression vector pLATE11 (aLICator Ligation Independent Cloning and Expression System; Thermo Scientific, Waltham, MA, USA). The amplification by PCR produced the correct expected band for each clone. The recombinant clones were checked by PCR colony screening and sequenced for a further confirmation. The positive clones were then transformed into competent BL21 (DE3) *E. coli* strain containing the T7RNA polymerase gene under the control of the isopropyl thio-β-D-galactoside-inducible lacUV5 promoter. Protein expression was carried on at 25 °C in LB medium containing 100 μg·mL^{-1} ampicillin and 5 μg·mL^{-1} hemin solution for all the species. Expression was induced by 0.5 mM isopropyl thio-β-D-galactoside. After 14–18 h, the reddish bacteria were collected by centrifugation and resuspended in 25 mM Tris (pH 8) and 10 mM EDTA. Cells were disrupted by sonication using a Microson ultrasonic cell disruptor (Misonix, Inc., Farmingdale, NY, USA) performing 10 cycles of 1 min each maintaining the cells in ice to avoid protein denaturation. Cell debris was removed by centrifugation for 10 min at 15000 ***g*** at 4 °C collecting the supernatant that contained the protein solution. hNgb was then precipitated in the presence of 4 M $(NH_4)_2SO_4$ and, after a proper salting out procedure by two dialysis changes, purified by anionic-exchange chromatography (DE-52; Whatman, Little Chalfont, UK) followed by a size-exclusion chromatography (Superdex G-75; GE Healthcare Life Sciences, Piscataway, NJ, USA) using an AKTA prime GE Healthcare system [56]. Approximately 8 mg of pure hNgb were obtained from 1 L of culture. The purity and the concentration of the proteins was tested by SDS gel electrophoresis (15% acrylamide), which yielded a single band in the gel at around 17 kDa for all of the sample testeds corresponding to the calculated neuroglobin masses [2,10,23].

Spectroscopic measurements

Electronic absorption spectra were recorded with a model V-570 spectrophotometer (Jasco, Tokyo, Japan). All experiments were carried out at 25 °C with 3–5 μM protein solutions freshly prepared before use in 10 mM phosphate buffer plus 0.1 M NaCl (pH 7.4). The protein concentration was checked spectrophotometrically using ε_{412} = 129 000 M^{-1}·cm^{-1} for all the proteins [44]. Hydrogen peroxide was added to the above solution to a final concentration of 50 and 200 μM. The experiments were repeated at least five times and the average kinetic constants for H_2O_2-induced heme degradation were affected by an uncertainty of ±0.005 h^{-1} (maximum deviation).

ThT fluorescence spectra for wt and mutated hNgb were obtained with a model FP-6000 spectrofluorimeter (Jasco). The spectra were recorded between 460 and 600 nm with excitation at 450 nm. Protein solutions, typically 3–5 μM, were made in 10 mM phosphate buffer plus 0.1 M NaCl (pH 7.4). Hydrogen peroxide was added to the above

solution to a final concentration of 200 μM. ThT was added to the protein solution 10 min prior to fluorescence measurements aiming to minimize the possible interaction with H_2O_2. However, no fluorescence emission signal is observed in the range 480–490 nm (excitation at 450 nm) when ThT is mixed with H_2O_2. Also in this case, the experiments were performed at least five times and kinetic constants for H_2O_2-induced nucleation (k_1) and autocatalytic growth at a surface (k_2) were calculated by fitting the Finke–Watzky model [72,73] and comprise average values, with the associated errors being the maximum deviations as above.

ATR-FTIR spectra were collected on a model FT-IR 4700 spectrophotometer (Jasco) equipped with the ATR reflection device ATR Pro One (Jasco). The samples were obtained by dialysis to remove the buffer and NaCl and treated with 200 μM H_2O_2 for 24 h. Ten microlitres of the solution was then deposited on ATR device and dried before the measurement.

AFM measurements were carried out in the tapping mode, on the same solutions used for the fluorescence spectra, which were deposited on a mica foil and air-dried at room temperature for 10–15 min. Protein samples (5 μM in 10 mM phosphate buffer plus 0.1 M NaCl, pH 7.4, and eventually 200 μM H_2O_2) were aged at 20 °C in the dark for 24 h. Approximately 20 μL of diluted sample (1 : 100) was deposited onto the freshly cleaved Mg^{2+} treated mica surfaces at room temperature (approximately 25 °C). The sample was incubated for 10 min in a water vapour saturated environment, then rinsed with ultrapure water and finally dried and stored in a flow of ultrapure dry nitrogen for at least 30 min at room temperature to remove the presence of water molecules at the surface.

The AFM analysis was performed by using a Multimode Nanoscope III atomic force microscope (Digital Instruments, Santa Barbara, CA, USA) with a Nanonis AFM control system (Nanonis – SPECS Zurich GmbH, Zurich, Switzerland) equipped with two oscillation controller modules (with digitally integrated phase-locked loop/lock-in). A nPoint closed-loop multimode scanner (nPoint, Inc., Madison, WI, USA) with a C-300 DSP closed-loop controller was used as fine actuator of the tip–sample relative motion. Bruker (Camarillo, CA, USA) RTESPA-150 and Nanoworld (Neuchâtel, Switzerland) Arrow-EFM type rectangular probes working in intermittent contact mode were used for the morphological characterization.

Computational analysis

The structures of the Ngb mutants were calculated by homology modelling using the SWISS-MODEL workspace [109], with the crystal structure of human neuroglobin (4mpm.pdb, chain A [12]) serving as a template, and used for calculations for the wt species. The volume of the heme cavity for each Ngb species was estimated using CASTP [110]. Note that the cavity volume calculation neglects the heme center.

Acknowledgements

This work was supported by the University of Modena and Reggio Emilia FAR2020 DSCG (MB), FAR2020 DSV (MS), FAR2020 Impulso and FAR2021 DSCG (GB) funding programs. Open Access Funding provided by Universita degli Studi di Modena e Reggio Emilia within the CRUI-CARE Agreement.

Conflict of interest

The authors declare no conflict of interest.

Author contributions

GDR and FB performed the experiments. GDR, FB, GB, AR and MB analyzed data. GB, AR and MB planned the experiments. GB, AR, CAR, MB and MS wrote the paper.

Data availability statement

The data presented in this study are available on request from the corresponding authors.

References

1 Brittain T. The anti-apoptotic role of neuroglobin. *Cells*. 2012;**1**:1133–55.
2 Ascenzi P, di Masi A, Leboffe L, Fiocchetti M, Nuzzo MT, Brunori M, et al. Neuroglobin: from structure to function in health and disease. *Mol Aspects Med*. 2016;**52**:1–48.
3 Vinogradov SN, Moens L. Diversity of globin function: enzymatic, transport, storage, and sensing. *J Biol Chem*. 2008;**283**:8773–7.
4 Fordel E, Thijs L, Moens L, Dewilde S. Neuroglobin and cytoglobin expression in mice: evidence for a correlation with reactive oxygen species scavenging. *FEBS J*. 2007;**274**:1312–7.
5 Jin K, Mao XO, Xie L, Khan AA, Greenberg DA. Neuroglobin protects against nitric oxide toxicity. *Neurosci Lett*. 2008;**430**:135–7.
6 Li RC, Morris MW, Lee SK, Pouranfar F, Wang Y, Gozal D. Neuroglobin protects PC12 cells against oxidative stress. *Brain Res*. 2008;**1190**:159–66.
7 Liu J, Yu Z, Guo S, Lee SR, Xing C, Zhang C, et al. Effects of neuroglobin overexpression on mitochondrial function and oxidative stress following hypoxia/reoxygenation in cultured neurons. *J Neurosci Res*. 2009;**87**:164–70.
8 Yu Z, Xu J, Liu N, Wang Y, Li X, Pallast S, et al. Mitochondrial distribution of neuroglobin and its response to oxygen-glucose deprivation in primary-

cultured mouse cortical neurons. *Neuroscience*. 2012;**218**:235–42.
9 Ascenzi P, Gustincich S, Marino M. Mammalian nerve globins in search of functions. *IUBMB Life*. 2014;**66**:268–76.
10 Dewilde S, Kiger L, Burmester T, Hankeln T, Baudin-Creuza V, Aerts T, et al. Biochemical characterization and ligand binding properties of neuroglobin, a novel member of the globin family. *J Biol Chem*. 2001;**276**:38949–55.
11 Kriegl JM, Bhattacharyya AJ, Nienhaus K, Deng P, Minkow O, Nienhaus GU. Ligand binding and protein dynamics in neuroglobin. *Proc Natl Acad Sci USA*. 2002;**99**:7992–7.
12 Guimarães BG, Hamdane D, Lechauve C, Marden MC, Golinelli-Pimpaneau B. The crystal structure of wild-type human brain neuroglobin reveals flexibility of the disulfide bond that regulates oxygen affinity. *Acta Crystallogr Sect D Biol Crystallogr*. 2014;**70**:1005–14.
13 Pesce A, Dewilde S, Nardini M, Moens L, Ascenzi P, Hankeln T, et al. Human brain neuroglobin structure reveals a distinct mode of controlling oxygen affinity. *Structure*. 2003;**11**:1087–95.
14 Arcovito A, Moschetti T, D'Angelo P, Mancini G, Vallone B, Brunori M, et al. An X-ray diffraction and X-ray absorption spectroscopy joint study of neuroglobin. *Arch Biochem Biophys*. 2008;**475**:7–13.
15 Schmidt M, Giessl A, Laufs T, Hankeln T, Wolfrum U, Burmester T. How does the eye breathe? Evidence for neuroglobin-mediated oxygen supply in the mammalian retina. *J Biol Chem*. 2003;**278**:1932–5.
16 Brunori M, Vallone B. A globin for the brain. *FASEB J*. 2006;**20**:2192–7.
17 De Marinis E, Marino M, Ascenzi P. Neuroglobin, estrogens, and neuroprotection. *IUBMB Life*. 2011;**63**:140–5.
18 Emara M, Turner AR, Allalunis-Turner J. Hypoxic regulation of cytoglobin and neuroglobin expression in human normal and tumor tissues. *Cancer Cell Int*. 2010;**10**:1–16.
19 Greenberg DA, Jin K, Khan AA. Neuroglobin: an endogenous neuroprotectant. *Curr Opin Pharmacol*. 2008;**8**:20–4.
20 Trent JT, Watts RA, Hargrove MS. Human neuroglobin, a hexacoordinate hemoglobin that reversibly binds oxygen. *J Biol Chem*. 2001;**276**:30106–10.
21 Lechauve C, Augustin S, Roussel D, Sahel JA, Corral-Debrinski M. Neuroglobin involvement in visual pathways through the optic nerve. *Biochim Biophys Acta*. 2013;**1834**:1772–8.
22 Wystub S, Laufs T, Schmidt M, Burmester T, Maas U, Saaler-Reinhardt S, et al. Localization of neuroglobin protein in the mouse brain. *Neurosci Lett*. 2003;**346**:114–6.
23 Burmester T, Weich B, Reinhardt S, Hankeln T. A vertebrate globin expressed in the brain. *Nature*. 2000;**407**:520–3.
24 Fago A, Mathews AJ, Brittain T. A role for neuroglobin: resetting the trigger level for apoptosis in neuronal and retinal cells. *IUBMB Life*. 2008;**60**:398–401.
25 Oleksiewicz U, Liloglou T, Field JK, Xinarianos G. Cytoglobin: biochemical, functional and clinical perspective of the newest member of the globin family. *Cell Mol Life Sci*. 2011;**68**:3869–83.
26 Lin Y, Cai B, Xue X-H, Fang L, Wu Z-Y, Wang N. TAT-mediated delivery of neuroglobin attenuates apoptosis induced by oxygen–glucose deprivation via the Jak2/Stat3 pathway in vitro. *Neurol Res*. 2015;**37**:531–8.
27 Moens L, Dewilde S. Globins in the brain. *Nature*. 2000;**407**:461–2.
28 Ostojić J, Sakaguchi DS, De Lathouder Y, Hargrove MS, Trent JT, Kwon YH, et al. Neuroglobin and cytoglobin: oxygen-binding proteins in retinal neurons. *Investig Ophthalmol Vis Sci*. 2006;**47**:1016–23.
29 Yu Z, Fan X, Lo EH, Wang X. Neuroprotective roles and mechanisms of neuroglobin. *Neurol Res*. 2009;**31**:122–7.
30 Wu F, Hu Z, Xu J, Tian Y, Wang L, Xian Y, et al. Immobilization of horseradish peroxidase on self-assembled (3-mercaptopropyl)trimethoxysilane film: characterization, direct electrochemistry, redox thermodynamics and biosensing. *Electrochim Acta*. 2008;**53**:8238–44.
31 Yu Z, Poppe JL, Wang X. Mitochondrial mechanisms of neuroglobin's neuroprotection. *Oxid Med Cell Longev*. 2013;**2013**:756989.
32 Lee S, Van Bergen NJ, Kong GY, Chrysostomou V, Waugh HS, O'Neill EC, et al. Mitochondrial dysfunction in glaucoma and emerging bioenergetic therapies. *Exp Eye Res*. 2011;**93**:204–12.
33 Sun Y, Jin K, Mao XO, Xie L, Peel A, Childs JT, et al. Effect of aging on neuroglobin expression in rodent brain. *Neurobiol Aging*. 2005;**26**:275–8.
34 Khan AA, Xiao OM, Banwait S, Jin K, Greenberg DA. Neuroglobin attenuates β-amyloid neurotoxicity in vitro and transgenic Alzheimer phenotype in vivo. *Proc Natl Acad Sci USA*. 2007;**104**:19114–9.
35 Sun F, Mao XO, Xie L, Greenberg DA, Jin K. Neuroglobin protein is upregulated in Alzheimer's disease. *J Alzheimers Dis*. 2013;**36**:659–63.
36 Chen LM, Xiong YS, Kong FL, Qu M, Wang Q, Chen XQ, et al. Neuroglobin attenuates Alzheimer-like tau hyperphosphorylation by activating Akt signaling. *J Neurochem*. 2012;**120**:157–64.
37 Brunori M, Giuffrè A, Nienhaus K, Nienhaus GU, Scandurra FM, Vallone B. Neuroglobin, nitric oxide,

and oxygen: functional pathways and conformational changes. *Proc Natl Acad Sci USA*. 2005;**102**:8483–8.
38 Herold S, Fago A, Weber RE, Dewilde S, Moens L. Reactivity studies of the Fe(III) and Fe(II)NO forms of human neuroglobin reveal a potential role against oxidative stress. *J Biol Chem*. 2004;**279**:22841–7.
39 Petersen MG, Dewilde S, Fago A. Reactions of ferrous neuroglobin and cytoglobin with nitrite under anaerobic conditions. *J Inorg Biochem*. 2008;**102**:1777–82.
40 Tejero J, Gladwin MT. The globin superfamily: functions in nitric oxide formation and decay. *Biol Chem*. 2014;**395**:631–9.
41 Trashin S, de Jong M, Luyckx E, Dewilde S, De Wael K. Electrochemical evidence for neuroglobin activity on NO at physiological concentrations. *J Biol Chem*. 2016;**291**:18959–66.
42 Tiso M, Tejero J, Basu S, Azarov I, Wang X, Simplaceanu V, et al. Human neuroglobin functions as a redox-regulated nitrite reductase. *J Biol Chem*. 2011;**286**:18277–89.
43 Tejero J, Sparacino-Watkins CE, Ragireddy V, Frizzell S, Gladwin MT. Exploring the mechanisms of the reductase activity of neuroglobin by site-directed mutagenesis of the heme distal pocket. *Biochemistry*. 2015;**54**:722–33.
44 Nicolis S, Monzani E, Ciaccio C, Ascenzi P, Moens L, Casella L. Reactivity and endogenous modification by nitrite and hydrogen peroxide: does human neuroglobin act only as a scavenger? *Biochem J*. 2007;**407**:89–99.
45 Tai H, Mikami S, Irie K, Watanabe N, Shinohara N, Yamamoto Y. Role of a highly conserved electrostatic interaction on the surface of cytochrome c in control of the redox function. *Biochemistry*. 2010;**49**:42–8.
46 Raychaudhuri S, Skommer J, Henty K, Birch N, Brittain T. Neuroglobin protects nerve cells from apoptosis by inhibiting the intrinsic pathway of cell death. *Apoptosis*. 2010;**15**:401–11.
47 Fago A, Mathews AJ, Moens L, Dewilde S, Brittain T. The reaction of neuroglobin with potential redox protein partners cytochrome b5 and cytochrome c. *FEBS Lett*. 2006;**580**:4884–8.
48 Bønding SH, Henty K, Dingley AJ, Brittain T. The binding of cytochrome c to neuroglobin: a docking and surface plasmon resonance study. *Int J Biol Macromol*. 2008;**43**:295–9.
49 Brittain T, Skommer J, Henty K, Birch N, Raychaudhuri S. A role for human neuroglobin in apoptosis. *IUBMB Life*. 2010;**62**:878–85.
50 Watanabe S, Wakasugi K. Neuroprotective function of human neuroglobin is correlated with its guanine nucleotide dissociation inhibitor activity. *Biochem Biophys Res Commun*. 2008;**369**:695–700.
51 Zanetti Polzi L, Battistuzzi G, Borsari M, Pignataro M, Paltrinieri L, Daidone I, et al. Computational investigation of the electron transfer complex between neuroglobin and cytochrome c. *Supramol Chem*. 2017;**29**:846–52.
52 Chen SF, Liu XC, Xu JK, Li L, Lang JJ, Wen GB, et al. Conversion of human neuroglobin into a multifunctional peroxidase by rational design. *Inorg Chem*. 2021;**60**:2839–45.
53 Chen L, Xu J-K, Li L, Gao S-Q, Wen G-B, Lin Y-W. Design and engineering of neuroglobin to catalyze the synthesis of indigo and derivatives for textile dyeing. *Mol Syst Des Eng*. 2022;**7**:239–47.
54 Hofbauer S, Pignataro M, Borsari M, Bortolotti CA, Di Rocco G, Ravenscroft G, et al. Pseudoperoxidase activity, conformational stability, and aggregation propensity of the His98Tyr myoglobin variant: implications for the onset of myoglobinopathy. *FEBS J*. 2022;**289**:1105–17.
55 Bocahut A, Derrien V, Bernad S, Sebban P, Sacquin-Mora S, Guittet E, et al. Heme orientation modulates histidine dissociation and ligand binding kinetics in the hexacoordinated human neuroglobin. *J Biol Inorg Chem*. 2013;**18**:111–22.
56 Bellei M, Bortolotti CA, Di Rocco G, Borsari M, Lancellotti L, Ranieri A, et al. The influence of the Cys46/Cys55 disulfide bond on the redox and spectroscopic properties of human neuroglobin. *J Inorg Biochem*. 2018;**178**:70–86.
57 Reeder BJ. Redox and peroxidase activities of the hemoglobin superfamily: relevance to health and disease. *Antioxid Redox Signal*. 2016;**26**:763–76.
58 Vinck E, Van Doorslaer S, Dewilde S, Moens L. Structural change of the heme pocket due to disulfide bridge formation is significantly larger for neuroglobin than for cytoglobin. *J Am Chem Soc*. 2004;**126**:4516–7.
59 Morozov AN, Roach JP, Kotzer M, Chatfield DC. A possible mechanism for redox control of human neuroglobin activity. *J Chem Inf Model*. 2014;**54**:1997–2003.
60 Astudillo L, Bernad S, Derrien V, Sebban P, Miksovska J. Probing the role of the internal disulfide bond in regulating conformational dynamics in neuroglobin. *Biophys J*. 2010;**99**:16–8.
61 Ishikawa H, Finkelstein IJ, Kim S, Kwak K, Chung JK, Wakasugi K, et al. Neuroglobin dynamics observed with ultrafast 2D-IR vibrational echo spectroscopy. *Proc Natl Acad Sci USA*. 2007;**104**:16116–21.
62 Ezhevskaya M, Trandafir F, Moens L, Dewilde S, Van Doorslaer S. EPR investigation of the role of B10 phenylalanine in neuroglobin – evidence that B10Phe mediates structural changes in the heme region upon disulfide-bridge formation. *J Inorg Biochem*. 2011;**105**:1131–7.
63 Picotti P, Dewilde S, Fago A, Hundahl C, De Filippis V, Moens L, et al. Unusual stability of human

neuroglobin at low pH – molecular mechanisms and biological significance. *FEBS J*. 2009;**276**:7027–39.
64 Hamdane D, Kiger L, Dewilde S, Green BN, Pesce A, Uzan J, et al. Coupling of the heme and an internal disulfide bond in human neuroglobin. *Micron*. 2004;**35**:59–62.
65 Bocahut A, Bernad S, Sebban P, Sacquin-Mora S. Relating the diffusion of small ligands in human neuroglobin to its structural and mechanical properties. *J Phys Chem B*. 2009;**113**:16257–67.
66 Hamdane D, Kiger L, Dewilde S, Green BN, Pesce A, Uzan J, et al. The redox state of the cell regulates the ligand binding affinity of human neuroglobin and cytoglobin. *J Biol Chem*. 2003;**278**:51713–21.
67 Skommer J, Helbo S, Henty K, Brittain T. Ligand binding, reactivity and biological activity of a distal pocket mutant of neuroglobin. *Int J Biol Macromol*. 2012;**51**:284–90.
68 Uno T, Ryu D, Tsutsumi H, Tomisugi Y, Ishikawa Y, Wilkinson AJ, et al. Residues in the distal heme pocket of neuroglobin: implications for the multiple ligand binding steps. *J Biol Chem*. 2004;**279**:5886–93.
69 Xu J, Yin G, Du W. Distal mutation modulates the heme sliding in mouse neuroglobin investigated by molecular dynamics simulation. *Proteins*. 2011;**79**:191–202.
70 Nienhaust K, Kriegl JM, Nienhaust GU. Structural dynamics in the active site of murine neuroglobin and its effects on ligand binding. *J Biol Chem*. 2004;**279**:22944–52.
71 Uppal S, Singh AK, Arya R, Tewari D, Jaiswal N, Kapoor A, et al. Phe28B10 induces channel-forming cytotoxic amyloid fibrillation in human neuroglobin, the brain-specific hemoglobin. *Biochemistry*. 2016;**55**:6832–47.
72 Watzky MA, Finke RG. Transition metal nanocluster formation kinetic and mechanistic studies. A new mechanism when hydrogen is the reductant: slow, continuous nucleation and fast autocatalytic surface growth. *J Am Chem Soc*. 1997;**119**:10382–400.
73 Morris AM, Watzky MA, Agar JN, Finke RG. Fitting neurological protein aggregation kinetic data via a 2-step, minimal/"Ockham's razor" model: the Finke-Watzky mechanism of nucleation followed by autocatalytic surface growth. *Biochemistry*. 2008;**47**:2413–27.
74 Du W, Syvitski R, Dewilde S, Moens L, La Mar GN. Solution 1H NMR characterization of equilibrium heme orientational disorder with functional consequences in mouse neuroglobin. *J Am Chem Soc*. 2003;**125**:8080–1.
75 Sies H. Hydrogen peroxide as a central redox signaling molecule in physiological oxidative stress: oxidative eustress. *Redox Biol*. 2017;**11**:613–9.
76 Barth A. Infrared spectroscopy of proteins. *Biochim Biophys Acta Bioenerg*. 2007;**1767**:1073–101.
77 Krimm S, Bandekar J. Vibrational spectroscopy and conformation of peptides, polypeptides, and proteins. In: Anfinsen CB, Edsall JT, Richards FMBT, editors. Advances in protein chemistry. Cambridge, MA: Academic Press; 1986. p. 181–364.
78 Surewicz WK, Mantsch HH. New insight into protein secondary structure from resolution-enhanced infrared spectra. *Biochim Biophys Acta*. 1988;**952**:115–30.
79 Sarroukh R, Goormaghtigh E, Ruysschaert J-M, Raussens V. ATR-FTIR: a "rejuvenated" tool to investigate amyloid proteins. *Biochim Biophys Acta*. 2013;**1828**:2328–38.
80 Gade Malmos K, Blancas-Mejia LM, Weber B, Buchner J, Ramirez-Alvarado M, Naiki H, et al. ThT 101: a primer on the use of thioflavin T to investigate amyloid formation. *Amyloid*. 2017;**24**:1–16.
81 Biancalana M, Koide S. Molecular mechanism of thioflavin-T binding to amyloid fibrils. *Biochim Biophys Acta*. 2010;**1804**:1405–12.
82 Antonini E, Brunori M. Hemoglobin and myoglobin in their reactions with ligands. Amsterdam: North Holland Publishing Company; 1967.
83 George P, Irvine DH. Reaction of metmyoglobin with hydrogen peroxide. *Nature*. 1951;**168**:164–5.
84 Svistunenko DA, Reeder BJ, Wankasi MM, Silaghi-Dumitrescu RL, Cooper CE, Rinaldo S, et al. Reaction of *Aplysia limacina* metmyoglobin with hydrogen peroxide. *Daltons Trans*. 2007;840–50. https://doi.org/10.1039/b615770j
85 Matsui T, Ozaki SI, Watanabe Y. On the formation and reactivity of compound I of the His-64 myoglobin mutants. *J Biol Chem*. 1997;**272**:32735–8.
86 Egawa T, Shimada H, Ishimura Y. Formation of compound I in the reaction of native myoglobins with hydrogen peroxide. *J Biol Chem*. 2000;**275**: 34858–66.
87 Khan KK, Mondal MS, Padhy L, Mitra S. The role of distal histidine in peroxidase activity of myoglobin transient-kinetics study of the reaction of H_2O_2 with wild-type and distal- histidine-mutanted recombinant human myoglobin. *Eur J Biochem*. 1998;**257**:547–55.
88 Brittain T, Baker AR, Butler CS, Little RH, Lowe DJ, Greenwood C, et al. Reaction of variant sperm-whale myoglobins with hydrogen peroxide: the effects of mutating a histidine residue in the haem distal pocket. *Biochem J*. 1997;**326**:109–15.
89 Ascenzi P, Leboffe L, Santucci R, Coletta M. Ferric microperoxidase-11 catalyzes peroxynitrite isomerization. *J Inorg Biochem*. 2015;**144**:56–61.
90 Mathai C, Jourd'heuil FL, Lopez-Soler RI, Jourd'heuil D. Emerging perspectives on cytoglobin, beyond NO dioxygenase and peroxidase. *Redox Biol*. 2020;**32**:101468.
91 Li D, Chen XQ, Li WJ, Yang YH, Wang JZ, Yu ACH. Cytoglobin up-regulated by hydrogen peroxide

plays a protective role in oxidative stress. *Neurochem Res*. 2007;**32**:1375–80.
92 Kawada N, Kristensen DB, Asahina K, Nakatani K, Minamiyama Y, Seki S, et al. Characterization of a stellate cell activation-associated protein (STAP) with peroxidase activity found in rat hepatic stellate cells. *J Biol Chem*. 2001;**276**:25318–23.
93 Hodges NJ, Innocent N, Dhanda S, Graham M. Cellular protection from oxidative DNA damage by over-expression of the novel globin cytoglobin in vitro. *Mutagenesis*. 2008;**23**:293–8.
94 Lardinois OM, Tomer KB, Mason RP, Deterding LJ. Identification of protein radicals formed in the human neuroglobin-H_2O_2 reaction using immuno-spin trapping and mass spectrometry. *Biochemistry*. 2008;**47**:10440–8.
95 King NK, Winfield ME. The mechanism of metmyoglobin oxidation. *J Biol Chem*. 1963;**238**:1520–8.
96 Li D, Zhang X, Long Y, Sun X. Inactivation of hemoglobin by hydrogen peroxide and protection by a reductant substrate. *Life Sci J*. 2006;**3**:52–8.
97 Cooper CE, Jurd M, Nicholls P, Wankasi MM, Svistunenko DA, Reeder BJ, et al. On the formation, nature, stability and biological relevance of the primary reaction intermediates of myoglobins with hydrogen peroxide. *Dalton Trans*. 2005;3483–8. https://doi.org/10.1039/b505786h
98 Nagababu E, Rifkind JM. Reaction of hydrogen peroxide with ferrylhemoglobin: superoxide production and heme degradation. *Biochemistry*. 2000;**39**:12503–11.
99 George P, Irvine DH. The higher oxidation state of metmyoglobin. *Biochem J*. 1953;**53**:xxv–xi.
100 Howes BD, Rodriguez-Lopez JN, Smith AT, Smulevich G. Mutation of distal residues of horseradish peroxidase: influence on substrate binding and cavity properties. *Biochemistry*. 1997;**36**:1532–43.
101 Liu Y, Moënne-Loccoz P, Loehr TM, Ortiz De Montellano PR. Heme oxygenase-1, intermediates in verdoheme formation and the requirement for reduction equivalents. *J Biol Chem*. 1997;**272**:6909–17.
102 Bhattacharya K, Rank KB, Evans DB, Sharma SK. Role of cysteine-291 and cysteine-322 in the polymerization of human tau into Alzheimer-like filaments. *Biochem Biophys Res Commun*. 2001;**285**:20–6.
103 Li Y, Yan J, Zhang X, Huang K. Disulfide bonds in amyloidogenesis diseases related proteins. *Proteins*. 2013;**81**:1862–73.
104 Honda R. Role of the disulfide bond in prion protein amyloid formation: a thermodynamic and kinetic analysis. *Biophys J*. 2018;**114**:885–92.
105 Pignataro M, Di Rocco G, Lancellotti L, Bernini F, Subramanian K, Castellini E, et al. Phosphorylated cofilin-2 is more prone to oxidative modifications on Cys39 and favors amyloid fibril formation. *Redox Biol*. 2020;**37**:101691.
106 MacPhee CE, Dobson CM. Formation of mixed fibrils demonstrates the generic nature and potential utility of amyloid nanostructures. *J Am Chem Soc*. 2000;**122**:12707–13.
107 Young LM, Tu LH, Raleigh DP, Ashcroft AE, Radford SE. Understanding co-polymerization in amyloid formation by direct observation of mixed oligomers. *Chem Sci*. 2017;**8**:5030–40.
108 Faravelli G, Mondani V, Mangione PP, Raimondi S, Marchese L, Lavatelli F, et al. Amyloid formation by globular proteins: the need to narrow the gap between in vitro and in vivo mechanisms. *Front Mol Biosci*. 2022;**9**:1–13.
109 Waterhouse A, Bertoni M, Bienert S, Studer G, Tauriello G, Gumienny R, et al. SWISS-MODEL: homology modelling of protein structures and complexes. *Nucleic Acids Res*. 2018;**46**:W296–303.
110 Tian W, Chen C, Lei X, Zhao J, Liang J. CASTp 3.0: computed atlas of surface topography of proteins. *Nucleic Acids Res*. 2018;**46**:W363–7.

Supporting information

Additional supporting information may be found online in the Supporting Information section at the end of the article.

Fig. S1. UV-visible spectra for wt hNgb without H_2O_2 (black line) and after 22 h of incubation with 200 μM H_2O_2 (red line).
Fig. S2. Soret bands for spectra of hNgb and variants recorded over time after addition of H_2O_2 50 μM (A to D) and 200 μM (E to H).
Fig. S3. Plot of the absorbance of the Soret band at 413 nm vs. time in the presence of 50 μM H_2O_2 (■) wt, (●) Y44A, (▲) Y44F, (×) K67A, (+) C46AC55A, (○) Y44A/C46A/C55A, (△) Y44F/C46A/C55A and (◆) K67A/C46A/C55A.
Fig. S4. ATR-FTIR spectra showing the Amide I and Amide II bands recorded over time after addition of H_2O_2 200 μM for (A) hNgb wt, (B) Y44A, (C) Y44F and (D) K67A mutant with (black lines) and without (C46AC55A mutations, red lines) disulfide bridge.
Fig. S5. Second-derivative ATR-FTIR spectra of the Amide I band recorded over time after addition of H_2O_2 200 μM for (A) hNgb wt, (B) Y44A, (C) Y44F and (D) K67A mutant with (black lines) and without (C46AC55A mutations, red lines) disulfide bridge.
Fig. S6. Morphological AFM images of protein aggregates formed by hNgb and variants subjected to incubation with H_2O_2: (A) wt, (B) C46AC55A, (C) Y44A, (D) Y44AC46AC55A, (E) Y44F, (F) Y44FC46AC55A, (G) K67A and (H) K67AC46AC55A.

Fig. S7. Topographic AFM images of protein aggregates formed by hNgb (a) wt, (b) C46AC55A, (c) Y44A, (d) Y44AC46AC55A, (e) Y44F, (f) Y44AC46AC55A, (g) K67A and (h) K67AC46AC55A subjected to incubation with H_2O_2 and section height of selected aggregates.

Fig. S8. Plot of k_{200} vs. the volume of the crevice where heme is placed (V_{hc}).

Fig. S9. Seecond derivative electronic absorption spectra of wt hNgb interacting with H_2O_2 at $t = 0$ (black) and after 6 h of incubation (red).